Ab initio calculation of the energy bands of (001) iron thin films*

Ed Caruthers, D. G. Dempsey, and Leonard Kleinman
Department of Physics, University of Texas, Austin, Texas 78712
(Received 22 March 1976)

Constructing a warped-muffin-tin potential from a superposition of $3d^7 4s^1$ atomic charge densities and the Slater exchange approximation, we have calculated the energy bands of a 13-layer (001) paramagnetic iron thin film using the supplemented orthogonalized-plane-wave method. The bands are compared with a previous parametrized linear combination of atomic orbitals calculation. Hybridized and unhybridized surface states are discussed and plots of wave functions of each kind are displayed. The planar average of the calculated charge is displayed and the possibility of a large d-electron contribution to the surface Friedel oscillation is discussed.

I. INTRODUCTION

Transition metals are generally less well understood and more difficult to perform calculations upon than simple metals and semiconductors. The d electrons are more localized about atomic sites than s and p electrons but atomic d orbitals do overlap and d bands do conduct. They can neither be treated as rigid core levels nor expanded in a few plane waves. Thus the methods used to study the electronic states at the surfaces of Li,[1] Na,[2] Al,[3] and Si,[4,5] are not applicable to the transition metals.

We have recently completed parametrized linear-combination-of-atomic-orbitals (LCAO) calculations of the energy bands of (100), (110), and (111) ferromagnetic iron[6] and copper[7] thin films. The parameters were determined from fits to bulk energy-band calculations and thus were quite adequate for the interior of the film. The parameters for surface atoms were varied, either to make the surface charge neutral or simply to observe the effect of such variation on the surface states. This method is useful as an initial study and if the surface parameters could be obtained by fitting a self-consistent *ab initio* thin-film calculation, it would be very useful in obtaining an accurate picture of the energy bands in films thicker than those amenable to *ab initio* calculations. This is desirable because some of the surface states found in iron[6] had decay lengths as large as 25 interplanar spacings. However, atomic orbitals are not capable of describing wave functions at and outside of the crystal surface. Thus the method is of no use in answering questions about the d-electron contribution to the surface Friedel oscillation or in making self-consistent calculations.

The method used by the Cambridge school[8,9] involves matching complex Bloch functions calculated in the bulk crystal potential with wave functions calculated in the external potential. The external potential is either taken to be a constant or to vary in the normal direction only. Thus there is an artificial discontinuity in the potential at the surface between the bulk and external regions. This method has never been used to calculate bulk states in the surface region. It has only been used to find surface states and since one must try to match bulk to vacuum wave functions separately for each $\bar{k}$ and E investigated, it is not unusual for some surface states to be overlooked. In the most extensive transition-metal calculations using this method,[10,11] surface states were found only in a narrow range of energies. Apparently only the s-d hybrid gap was investigated since a larger number of unhybridized and d-d hybridized surface states were not found.[7a]

There have recently been attempts to derive criteria for the existence of surface states.[11,12] We have shown however that no such criteria exist.[13] This fact is in agreement with our LCAO studies,[6,7] where we found that some surface states are not very sensitive to the exact surface potential (these are generally hybridized surface states) but that the existence of other surface states depends critically on the surface potential and that the number of surface states in a gap can vary over a large range (we found between zero and four). Thus to obtain an accurate description of the surface states one needs the correct, i.e., self-consistent potential. Self-consistent calculations are also needed to determine the d-electron contribution to the surface Friedel oscillation. The simple metals[1-3] show a charge oscillation which is a nonlinear sum of the jellium Friedel oscillation[14] and the bulk crystal oscillations. Because the jellium calculation shows the Friedel oscillations to be suppressed in a high-density electron gas, one might suspect that they will be weak in iron. However there is no *a priori* reason to believe that the jellium results will be applicable to transition metals.

Ab initio transition-metal thin film calculations

have been performed by Kasowski[15] using the muffin-tin-orbital method. It appears that this method might lend itself to self-consistent calculations but the only published results are not self-consistent and have, in fact, been limited to a single point in the two-dimensional Brillouin zone (2D BZ). Our recently reported calculation on 13-layer (001) paramagnetic iron[16] is the only other *ab initio* calculation of which we are aware. In this paper we extend that calculation to the same set of points in the 2D BZ that we used in our Al (Ref. 3a) and self-consistent Li (Ref. 1) calculations. In Sec. II we briefly describe the supplemented-OPW (orthogonalized plane wave) method[17] used in the calculation and describe in some detail the construction of the thin-film crystal potential. In Sec. III we display the energy bands in the 2D BZ and compare them with the LCAO bands. Many features are so insensitive to the potential that they are common to all three sets of bands (LCAO ferromagnetic majority- and minority-spin bands and supplemented-OPW paramagnetic bands) whereas others are not. Those features common to all three sets of bands undoubtably do exist in both paramagnetic and ferromagnetic iron (001) surfaces. We discuss the various surface states and plot the wave functions of typical unhybridized, slightly hybridized. and fully hybridized surface states. The density of states and the charge density are calculated. The planar average of the charge density is plotted and a huge Friedel peak obtained. Although the effect of self-consistency will be to suppress this peak, this calculation shows that the d electrons react even more strongly to the presence of the surface than do nearly free electrons. Thus in this paper we perform the first *ab initio* transition-metal thin-film energy-band calculation throughout the 2D BZ, we describe several specific features of the (001) iron surface electronic structure, and we obtain insight into the general characteristics of transition-metal surfaces. In addition we lay the groundwork for future self-consistent calculations.

II. METHOD

As for the simple metals[1,3] we take our (001) iron film to be 13 layers thick and add an empty selvage region three layers thick on both sides over which the wave functions are assumed to decay to zero. We take as basis functions

$$\phi_{ij}^{\pm}=2^{-1/2}(|\vec{k}+\vec{G}_i+\vec{k}_{3j}\rangle \pm |\vec{k}+\vec{G}_i-\vec{k}_{3j}\rangle), \tag{1}$$

where $\vec{k}$ is a wave vector lying within the 2D BZ, the $\vec{G}_i$ are two-dimensional (2D) reciprocal-lattice vectors, and $\vec{k}_3$ is a wave vector in the [001] direction. The $|\vec{k}+\vec{G}+\vec{k}_{3j}\rangle$ are plane waves $\Omega^{-1/2}\exp i[(\vec{k}+\vec{G}_i)\cdot\vec{r}+k_{3j}z]$, which have been orthogonalized to the five core functions ($1s, 2s, 2p, 3s$, $3p$) on each ion calculated in the spherically averaged thin film potential. (This spherically averaged potential is different for surface ions and for interior ions.) The normalization factor $\Omega=(\frac{19}{2}a)\times a\times a$. The k_{3j} are chosen so that the $\phi_{ij}^{\pm}$ are zero at the end of the selvage region, i.e., at $z=\pm\frac{19}{4}a$. Thus

$$k_{3j}=2j\pi/19a, \tag{2}$$

with j an odd integer for ϕ_{ij}^{+} and an even integer for ϕ_{ij}^{-}. As noted above the d electrons are too localized about atomic sites to be expanded in a few plane waves. (There being no d core levels, the OPW's reduce to plane waves for states with d symmetry.) Therefore we supplement the OPW's with a set of d planar Bloch functions

$$\phi_{n\alpha}^{\sigma}=2^{-1/2}\sum_i [F_{n\alpha}(\vec{r}-\vec{R}_i-\vec{\tau}_n-\vec{Z}_n) \pm F_{n\alpha}(\vec{r}-\vec{R}_i-\vec{\tau}_n+\vec{Z}_n)]e^{i\vec{k}\cdot\vec{R}_i}, \tag{3}$$

where R_i is a 2D lattice vector, $\vec{\tau}_n=0$ for n even (A plane) and $\vec{\tau}_n=(\frac{1}{2}a,\frac{1}{2}a)$ for n odd (B plane), $\vec{Z}_n$ is a vector of length $\frac{1}{2}na$ to the nth plane, and $F_{n\alpha}(\vec{r})=f_n(r)K_\alpha(\theta\phi)$. Here $f_n(r)$ is a radial function which vanishes with vanishing slope at the inscribed sphere radius and K_α is an $l=2$ cubic harmonic with α being xy, yz, zx, x^2-y^2, or $3z^2-r^2$. The superscript σ represents the reflection parity of $\phi_{n\alpha}^{\sigma}$ and is the same as the sign between the two $F_{n\alpha}$'s in Eq. (3) if α is even under change of sign of z, i.e., if $\alpha=xy$, x^2-y^2, or $3z^2-r^2$. If $\alpha=yz$ or zx, the sign of σ is reversed. On the central ($n=0$) plane we have

$$\phi_{0\alpha}^{\sigma}=\sum_i F_{0\alpha}(\vec{r}-\vec{R}_i)e^{i\vec{k}\cdot\vec{R}_i}, \tag{4}$$

where the parity of $\phi_{0\alpha}^{\sigma}$ is that of α. Thus we add 33 even and 32 odd basis functions[18] to our even and odd combinations of OPW's in Eq. (1). The radial functions f_n are calculated in the spherically averaged crystal potential (and hence are slightly different for different n) according to a prescription we have developed[17] which gives improved convergence, i.e., minimizes the number of OPW's needed in the expansion.

In this calculation we have used 23 k_{3j}'s for each parity and all $\vec{k}+\vec{G}_i$ such that $|\vec{k}+\vec{G}_i|\leq 5\pi/a$ at each $\vec{k}$. Planar symmetrized combinations of the OPW's are used to reduce the size of the secular equation and the symmetry can be used to reduce the number of d-basis functions as well. (See Table II of Ref. 6a for the d functions occurring in each irreducible representation at each symmetry point of the 2D BZ.) The largest matrix

diagonalized was a 319×319 Δ_1^+. It required 13 planar symmetrized combinations of the OPW's as well as $x^2 - y^2$, $3z^2 - r^2$ and xz d functions for a total of $13 \times 23 + 7 + 6 = 319$ basis functions. An estimate of the convergence in k_3 is obtained by noting that increasing the number of k_3 from 23 to 33 at $\bar{\Gamma}$ caused a drop of 0.006 Ry in one of the $\bar{\Gamma}_1$ levels. Nearby $\bar{\Gamma}_1$ levels dropped somewhat less and all other $\bar{\Gamma}$ levels dropped considerably less.

Our potential is constructed from a superposition of $3d^7 4s^1$ atomic charge densities obtained from a Herman-Skillman[19] calculation using the Slater[20] exchange approximation

$$V^{ex}(\vec{r}) = -3[3\rho(r)/\pi]^{1/3}. \tag{5}$$

To calculate this exchange in the thin film we divided the charge into two parts. The first consists of spherically averaged overlapped charged inside muffin-tin (MT) spheres of radius[21] $r_0 = 2.313$ a.u. This charge is generated by the Löwdin α-expansion method.[22] We calculate $\rho_{MT}^{1/3}(r)$ and $V_{MT}^{ex}(r)$ at 250 Herman-Skillman[19] radial mesh points,[23] $r \le r_0$. In principle, we should, and in practice we could, with considerably more effort, generate the exact $\rho_{MT}(\vec{r})$ and $\rho_{MT}^{1/3}(\vec{r})$ in an expansion of spherical harmonics. The $V_{MT}^{ex}(r)$ are Fourier transformed, multiplied by $\exp i(\bar{G} \cdot \bar{\tau}_n + k_3 Z_n)$, and added to obtain the thin film $V_{MT}^{ex}(\bar{G}, k_3)$. The remaining part of the charge is simply[24]

$$\rho_{out}(\vec{r}) = \sum_j \rho_{atom}(\vec{r} - \vec{R}_j) - \sum_j \rho_{MT}^j(\vec{r} - \vec{R}_j).$$

However, because of it discontinuity at the MT spheres, the Fourier expansion of $\rho_{out}(\vec{r})$ converges too slowly. Therefore, we define

$$\begin{aligned}\rho_s(\vec{r}) &= \bar{\rho}(\vec{r}) + \rho_{out}(\vec{r}) \\ &= \sum_j \rho_{atom}(\vec{r} - \vec{R}_j) \\ &\quad - \sum_j \rho_{MT}^j(\vec{r} - \vec{R}_j) + \sum_j \bar{\rho}_{MT}^j(\vec{r} - \vec{R}_j),\end{aligned} \tag{6}$$

where $\bar{\rho}_{MT}^j(\vec{r} - \vec{R}_j)$ is equal to $\rho_{MT}^j(r_0)$ when $|\vec{r} - \vec{R}_j| \le r_0$ and zero otherwise. Now $\rho_s(\vec{r})$, being a sum of spherical charge densities, is easily Fourier transformed to obtain $\rho_s(\bar{G}, k_3)$ and this is inverse Fourier transformed to obtain $\rho_s(\bar{G}, z)$. Because $\rho_s(\vec{r})$ is continuous and has no large peaks, $\rho_s(\bar{G} = 0, z)$ is much larger than $\rho_s(\bar{G} \ne 0, z)$ and we can use a Taylor series expansion to find the cube root of ρ_s:

$$\rho_s(\bar{r}, z) = \sum_{\bar{G}} \rho_s(\bar{G}, z) e^{i\bar{G} \cdot \bar{r}}, \tag{7}$$

$$[\rho_s(\bar{r}, z)]^{1/3} = \sum_{\bar{G}} A(\bar{G}, z) e^{i\bar{G} \cdot \bar{r}}, \tag{8}$$

$$V_s^{ex}(\bar{r}, z) = \sum_{\bar{G}} [-6(3/8\pi)^{1/3} A(\bar{G}, z)] e^{i\bar{G} \cdot \bar{r}}, \tag{9}$$

where the $A(\bar{G}, z)$ in (8) and (9) are given by

$$A(\bar{G} = 0, z) = [\rho_s(\bar{G} = 0, z)]^{1/3} \left(1 - \frac{1}{9} \sum_{\bar{G}}{}' [\hat{\rho}_s(\bar{G}, z)]^2\right) \tag{10}$$

and

$$\begin{aligned}A(\bar{G} \ne 0, z) &= [\rho_s(\bar{G} = 0, z)]^{1/3} \\ &\quad \times \left(\frac{1}{3} \hat{\rho}_s(\bar{G}, z) - \frac{1}{9} \sum_{\bar{G}'}{}' \hat{\rho}_s(\bar{G}', z) \hat{\rho}_s(\bar{G} - \bar{G}', z)\right),\end{aligned} \tag{11}$$

where $\hat{\rho}(\bar{G}, z) = \rho(\bar{G}, z)/\rho(G = 0, z)$ and the prime on the last sum indicates neither $\bar{G}'$ nor $\bar{G} - \bar{G}' = 0$. Then $V_{out}^{ex}(\bar{G}, k_3) = V_s^{ex}(\bar{G}, k_3) - \bar{V}^{ex}(\bar{G}, k_3)$ where $V_s^{ex}(\bar{G}, k_3)$ is obtained from Fourier transforming Eq. (9) and $\bar{V}^{ex}(\bar{G}, k_3)$ is easily obtained from $\bar{\rho}(\vec{r})$, a sum of spherical constant nonoverlapping charges. Note that, in general, one cannot add Slater exchange potentials because $(\rho_A + \rho_B)^{1/3} \ne \rho^{1/3} + \rho_B^{1/3}$ however neither $\bar{\rho}$ nor ρ_{MT} overlap ρ_{out} so $\rho_s^{1/3} = (\bar{\rho} + \rho_{out})^{1/3} = \bar{\rho}^{1/3} + \rho_{out}^{1/3}$, etc. Thus

$$V^{ex}(\bar{G}, k_3) = V_{MT}^{ex}(\bar{G}, k_e) + V_s^{ex}(\bar{G}, k_3) - \bar{V}^{ex}(\bar{G}, k_3). \tag{12}$$

The second-order terms in Eqs. (10) and (11) increased $V^{ex}(\bar{G}, k_3)$ from zero (large $\bar{G}, k_3$) to 0.0015 Ry ($\bar{G}, k_3 = 0$) in this calculation so that the largest errors in the expansion undoubtably arise from the replacement of $\rho_{MT}(\vec{r})$ by its spherical average. For smooth pseudocharge densities in simple metals it may be possible to calculate $\rho^{1/3}(\vec{r})$ on a fairly gross mesh of points in the $(\frac{19}{2}a) \times a \times a$ unit cell but such a procedure is not possible in a transition metal with its sharply peaked d functions. We have gone to so much trouble to develop and use this very accurate technique because it is directly applicable to self-consistent calculations, both thin film and bulk.

The $V^{Coul}(\bar{G} = 0, k_3 \to 0)$ are very sensitive to the large r tail of the atomic $4s$ charge density. There is no reason to expect this tail to be unchanged when the atoms are superposed to form the crystal. Therefore, we vary the large r part of $V_{4s}(r)$, the potential due to the $4s$ electron plus one proton, in the following way. We first calculate the Fourier transform $V_{4s}^{(0)}(K)$, change it smoothly for K small (compared to the smallest $\bar{G}$) so as to shift $V_{4s}(K = 0)$ by an estimate of the amount of necessary to obtain the correct work function[25] (in this case from -0.823 to -0.548 Ry) based on $\bar{\Gamma}$ energy levels calculated previously[16] in the unmodified potential. We then multiply $V_{4s}^{(1)}(K)$ by the structure factor to obtain the thin

film $V_{4s}^{(1)}(\bar{G}=0,k_3)$ which is Fourier transformed to obtain $V_{4s}^{(1)}(\bar{G}=0,z)$. This is adjusted for z in the selvage region to match the jellium Coulomb potential[14] for $r_s=2.66$ (i.e., jellium with a density of one electron per iron atomic volume). We take this $V_{4s}^{(2)}(\bar{G}=0,z)$ and Fourier transform back to obtain $V_{4s}^{(2)}(\bar{G}=0,k_3)$. The selvage region adjustment (large z) affects only small k_3's. Thus

$$V_{\text{final}}^{\text{Coul}}(\bar{G}=0,k_3)=V_{\text{initial}}^{\text{Coul}}(\bar{G}=0,k_3)+V_{4s}^{(2)}(\bar{G}=0,k_3)-V_{4s}^{(0)}(\bar{G}=0,k_3). \tag{13}$$

The other $V^{\text{Coul}}(\bar{G},k_3)$ are obtained simply by multiplying the atomic $V^{\text{Coul}}(K)$ by the thin-film structure factor. We obtain the $V_{\text{MT}}^{\text{Coul}}(r)$ from overlapping the atomic Coulomb potentials $V_{\text{initial}}^{\text{Coul}}(r)+\Delta V_{4s}(r)$ using the Löwdin α-expansion,[22] where $\Delta V_{4s}(r)$ is the Fourier transform of $\Delta V_{4s}(K)$ which is obtained by dividing $V_{4s}^{(2)}(\bar{G}=0,k_3)-V_{4s}^{(0)}(\bar{G}=0,k_3)$ by the structure factor. This method of adjusting the large-r small-K region of the superposed Coulomb potentials is almost identical to the way we adjusted the pseudopotential for aluminum[3] where it led to a calculated charge density which went smoothly from the correct bulk charge density to the correct jellium charge density in the selvage region.

III. 2D ENERGY BANDS

Since there are five $3d$ bands and one $4s$ band per atom and 13 atoms per thin-film unit cell, there are about 78 bands below the vacuum level. To make the bands more legible we separate them; the $\bar{\Delta}_1$, $\bar{Y}_1$, and $\bar{\Sigma}_1$ bands are shown in Fig. 1 and the $\bar{\Delta}_2$, $\bar{Y}_2$, and $\bar{\Sigma}_2$ bands in Fig. 2. Bands of the same 2D symmetry which cross one another have opposite parity. The energy range of all the symmetries at $\bar{\Gamma}$, $\bar{X}$, and $\bar{M}$ are shown in Figs. 1 and 2. This is necessary because of the connectivity relations (see Table I of Ref. 26), e.g., $\bar{\Gamma}_3$ connects

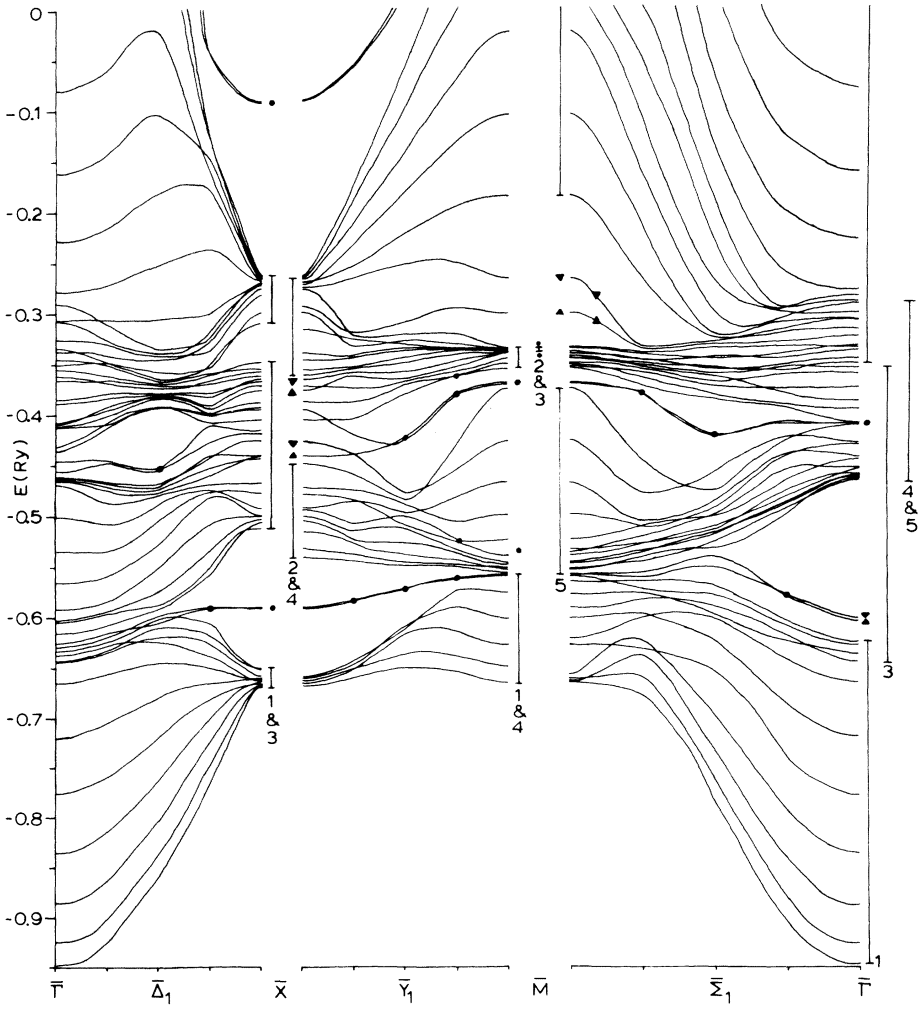

FIG. 1. 2D energy bands of $\bar{\Delta}_1$, $\bar{Y}_1$, and $\bar{\Sigma}_1$ symmetry for a 13-layer (001) iron thin film.

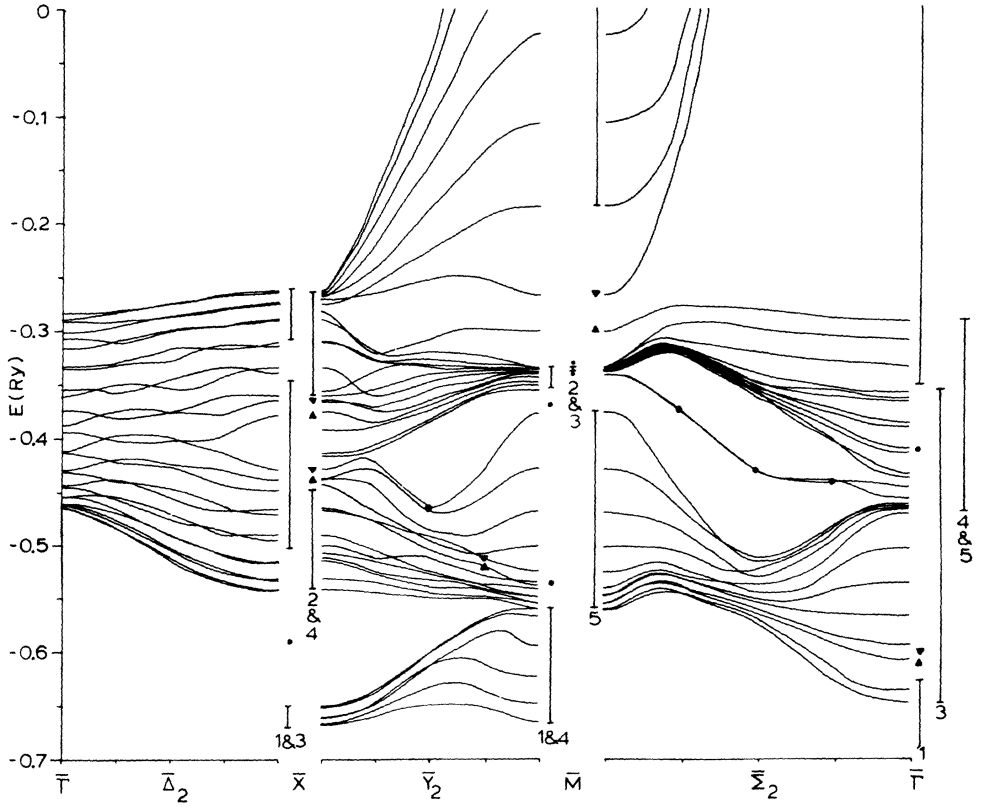

FIG. 2. 2D energy bands of $\bar{\Delta}_2$, $\bar{Y}_2$, and $\bar{\Sigma}_2$ symmetry for a 13-layer (001) iron thin film.

with $\bar{\Delta}_1$ and also with $\bar{\Sigma}_2$. Surface states occur in pairs with even and odd parity. For infinitely thick films these are degenerate and may be combined to form surface states localized on the opposite faces of the film. We designate nearly degenerate surface states in Figs. 1 and 2 by a dot. Where the decay length is longer and therefore the degeneracy more split we use a pair of triangles pointing toward one another.

Figure 3 shows the density of states calculated from these bands. The energy mesh is 0.01 Ry and each energy level was spread over 0.01 Ry and contributed to two energy intervals in proportion to its overlap. Each energy level, calculated at one of 12 points in the irreducible $\frac{1}{8}$ 2D BZ, was weighed by a factor nA/A_0, where n is the number of members of the star of $\bar{k}$, A_0 is the area of the 2D BZ, and A is the proximity area of $\bar{k}$ shown in Fig. 1 of Ref. 1. The Fermi energy determined from this density-of-states curve is −0.354 Ry or 4.81 eV so that our adjustment of the zeroth Fourier transform of $V_{4s}(r)$ was satisfactory in this respect.

We note that our bands are quite similar to those we projected[26,27] from Wood's[28] bulk band calculation. Our bands here are slightly narrower, but the major gaps are about where we projected them. Whether or not the narrow projected gaps exist here cannot be determined because those gap widths are of the same order as the spacing between bands in a 13-layer film. Our bands differ somewhat more from the LCAO ferromagnetic 41-layer thin-film bands,[6a] partly because of the ferromagnetism and partly because the LCAO parameters were obtained by fitting a bulk cal-

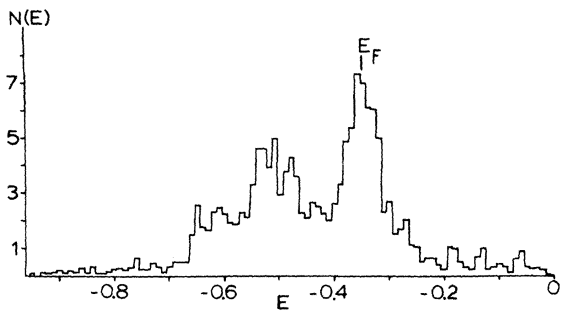

FIG. 3. Density of states for a 13-layer iron thin film in units of electrons per 2D unit cell per 10^{-2} Ry. The 2D unit cell contains 104 electrons.

culation[29] which used only 64% of the Slater exchange. But the differences between our results and the LCAO results are generally less than the differences between the LCAO majority and LCAO minority spin bands. Unless otherwise specified in the descriptions which follow, our gaps are the same as the larger LCAO gaps and corresponding gaps contain much the same surface states, or are empty, in the two cases.

The bottom of the highest gap sweeps upward from −0.26 Ry at $\bar{X}$ up to positive energies in the $\bar{\Delta}$ and $\bar{Y}$ directions. It contains a $\bar{\Delta}_1 - \bar{X}_1 - \bar{Y}_1$ surface state with a minimum of −0.09 Ry at $\bar{X}$. This is a nearly-free-electron surface state which also occurs in lithium.[1] It arises from a gap in the three-dimensional (3D) bands between a pure-p N_1, state lying just below the top of the d bands and an N_1 state lying in the vacuum which is nearly pure s with a very slight d admixture. The second $\bar{\Delta}_1$ gap at −0.33 Ry is widest at $\bar{X}$ where it becomes the $\bar{X}_{1,3}$ gap. Like the corresponding majority spin LCAO gap, it contains no surface state. The minority-spin LCAO gap contains two surface states but in a narrow tail of the gap which cannot be distinguished in the 13-layer film. The third $\bar{\Delta}_1$ gap is an s-d hybridizing gap and contains a surface state at an energy of about −0.45 Ry. This gap pinches off at $\bar{\Gamma}$ and about $\frac{3}{4}$ of the way to $\bar{X}$. Because it lies in a continuum of $\bar{\Delta}_2$ states, the $\bar{\Delta}_1$ surface state must become a resonance an infinitesimally small distance off the $\bar{\Delta}$ symmetry line. The fourth $\bar{\Delta}_1$ gap is also an s-d hybridizing gap. It runs from about $\frac{5}{8}$ of the way between $\bar{\Gamma}$ and $\bar{X}$ to $\bar{X}$ and then continues along the entire length of the $\bar{Y}$ line, pinching off at $\bar{M}$. It contains a $\bar{\Delta}_1 - \bar{X}_1 - \bar{Y}_1$ surface state (at about −0.59 Ry at $\bar{X}$), well centered in the gap which becomes less localized as the gap narrows and becomes completely bulklike at $\bar{M}$. There is a similar $\bar{Y}$ gap in the LCAO minority-spin bands but it is only half as wide and a $\bar{Y}_1$ surface state appears only briefly near the top of the gap. In the majority spin bands there is no $\bar{Y}$ gap near $\bar{X}$ and only a small gap appears in the middle of the $\bar{Y}$ line as a remnant of this gap; it contains a $\bar{Y}_2$ surface state. Along $\bar{\Delta}$, both LCAO spins have a gap similar to the one here. The single $\bar{\Delta}_2$ gap lies right in the middle of the d bands and arises from nonhybridizing bands in three dimensions. It is widest at $\bar{X}$ and pinches off $\frac{3}{8}$ of the way to $\bar{\Gamma}$. There is an $\bar{X}_4$ surface state at the top of the gap and an $\bar{X}_2$ at the bottom. They are not observed $\frac{1}{4}$ of the way to $\bar{\Gamma}$ and presumably have run into the continua of the top and bottom of the gap before that point. An $\bar{X}_4$ surface state with exactly the same behavior was observed for both spins in the LCAO calculation. The $\bar{X}_2$ surface state which initially existed in that calculation was pulled into the continuum by the shift in the atomic surface parameters needed to make the surface charge neutral.

Along $\bar{Y}$, the $\bar{Y}_1$ and $\bar{Y}_2$ bands are, except for surface states, very nearly identical and would become more so were the film thicker.[30] There are five $\bar{Y}_{1,2}$ gaps, the highest and lowest of which have already been discussed. The second highest gap runs from $\bar{M}$ (where it extends from the top of the $\bar{M}_{1,4}$ and $\bar{M}_{2,3}$ continua to the bottom of the second $\bar{M}_5$ continuum) to some ill defined point on the $\bar{Y}$ line. Because of the large spacing between the states at the top of the gap, the gap is considerably wider than it would be in a thicker film. A pair of $\bar{M}_5$ surface states whose degeneracy is split by over 0.03 Ry extends along $\bar{Y}$ with both $\bar{Y}_1$ and $\bar{Y}_2$ symmetry (all $\bar{M}_5$ levels are two-fold degenerate[31] and connect to both $\bar{Y}_1$ and $\bar{Y}_2$ states). The $\bar{M}_5$ surface state decay length was determined to be 25 interplanar spacings in a 321-layer LCAO calculation[6a] and is even larger along $\bar{Y}$. In the 13-layer film these $\bar{Y}$ surface states cannot be recognized as surface states and their splitting is even greater than at $\bar{M}$. We assume that in a thicker film where the splitting of the surface state would not obscure things, that the gap would extend all the way to $\bar{X}$ before pinching off. The gap continues along $\bar{\Sigma}$ as both a $\bar{\Sigma}_1$ and $\bar{\Sigma}_2$ gap. The $\bar{\Sigma}_1$ gap pinches off about $\frac{1}{4}$ of the way to $\bar{\Gamma}$ and contains a surface state which is less split and has a shorter decay length[32] than at $\bar{M}$. The $\bar{\Sigma}_2$ gap appears to open up very rapidly but a 321-layer LCAO calculation[6a] as well as a projection of Wood's bulk bands[27] shows that it pinches off about $\frac{1}{8}$ of the way to $\bar{\Gamma}$ and then reopens, becoming very wide at $\bar{\Gamma}$. The $\bar{\Sigma}_2$ surface state connecting to the $\bar{M}_5$ surface state is, of course, almost immediately obscured upon leaving $\bar{M}$ in the 13-layer film. These $\bar{Y}$ and $\bar{\Sigma}$ surface states exist for the minority spins but not the majority in the LCAO calculation. The third $\bar{Y}$ gap has its maximum width in the middle of $\bar{Y}$ and is narrower but still a gap at $\bar{M}$. This gap contains a $\bar{Y}_1$ surface state which runs the length of the gap to $\bar{M}$ (at −0.37 Ry) where it has $\bar{M}_1$ symmetry. It continues in the second $\bar{\Sigma}_1$ gap as a surface state more than $\frac{1}{2}$ way to $\bar{\Gamma}$. A second $\bar{Y}_1$ surface state exists right at the top of the gap about 25% of the way from $\bar{M}$ to $\bar{X}$ and immediately disappears into the bulk bands on both sides of this point. A single $\bar{Y}_2$ surface state exists at the bottom of the gap in the middle of the $\bar{Y}$ line and goes into the bulk bands on both sides of this point. In the LCAO calculations this pinches off before reaching $\bar{M}$ and contains no $\bar{Y}_2$ surface state although it does connect to the same $\bar{\Sigma}_1$ and $\bar{\Sigma}_2$ gaps through the interior of the 2D BZ. The fourth $\bar{Y}$ gap actually cannot be seen as such for the 13-layer film; how-

ever, a Y_1 and a Y_2 surface state are observed $\frac{1}{4}$ of the way from $\bar{M}$ to $\bar{X}$ at about -0.52 Ry. Examination of projected paramagnetic bulk bands[26] shows that this is an extremely narrow gap which pinches off at $\bar{M}$ because, in 3D, three bands become degenerate at P_4. It also pinches off about 30% of the way to $\bar{X}$ when a 3D indirect gap vanishes. In the ferromagnetic bands[6a] of both spins, this gap is much wider and extends 75% of the way to $\bar{X}$.

An $\bar{M}_4$ surface state at -0.53 Ry lies in the $\bar{M}_5$ continuum and, therefore, is completely isolated from any Y or Σ gaps. This surface state must become a resonance upon moving away from the $\bar{M}$ point in any direction in the 2D BZ. An $\bar{M}_2$ surface state lies only 0.0001 Ry above the top of the $\bar{M}_{2,3}$ continuum which itself is only 0.0025 Ry wide. Since the top of the $\bar{M}_{1,4}$ continuum appears to be degenerate with the top of the $\bar{M}_{2,3}$ continuum[33] this $\bar{M}_2$ surface state is in an absolute gap and must connect to Y_2 and Σ_2 surface states. These run into the bottom of the Y and Σ_2 gaps and are not observed $\frac{1}{4}$ of the way to $\bar{X}$ and $\bar{\Gamma}$. An $\bar{M}_3$ surface state whose degeneracy is split by only 0.00001 Ry lies 0.0029 Ry below the $\bar{M}_{2,3}$ continuum. Neither the $\bar{M}_2$ nor the $\bar{M}_3$ surface state existed in the original LCAO calculation but when the atomic surface parameters were made more negative the $\bar{M}_3$ surface state was pulled out of the continuum. This $\bar{M}_3$ surface state is the end point of a $\bar{\Sigma}_2$ surface state which runs almost to $\bar{\Gamma}$ where the very wide Σ_2 gap pinches off. Over the middle of the Σ_2 gap this is a highly hybridized surface state although it is not the usual s-d, but rather d-d hybridization. In the 3D bands one finds $\Gamma_{25'}$ lying below Γ_{12} but in the (001) corner of the BZ, $H_{25'}$ lies well above H_{12}. Thus as soon as one gets away from the Δ line connecting Γ and H where symmetry prevents the bands from hybridizing, one obtains a very strong t_{2g}-e_g hybridization. The lowest $\bar{\Sigma}_1$ gap has its maximum width at $\bar{\Gamma}$ and contains a $\bar{\Sigma}_1 - \bar{\Gamma}_1$ surface state a little above the bottom of the gap at about -0.59 Ry. Even at $\bar{\Gamma}$ this surface state has a moderately long attenuation length and it disappears as the gap pinches off about 45% of the way to $\bar{M}$. This is a classical s-d hybridization gap which gets narrower in going away from $\bar{\Gamma}$. It probably pinches off as the 3D gap becomes indirect and bands of the same symmetry overlap. In our projection,[26] however, the 3D gap remained direct and the 2D gap only pinched off at $\bar{M}$ as the 3D bands became degenerate at P_4. Because the $\bar{\Gamma}_1$ gap is completely overlapped by $\bar{\Gamma}_3$ bands, neither the $\bar{\Sigma}_1$ gap or its surface states exist off the $\bar{\Sigma}$ direction. Finally, there is a well-localized $\bar{\Gamma}_1$ surface state at -0.41 Ry. Because it is overlapped by both $\bar{\Gamma}_3$ and $\bar{\Gamma}_{4,5}$ continua, it cannot exist as a surface state except right at $\bar{\Gamma}$. It appears to connect with a $\bar{\Sigma}_1$ state which becomes a surface state halfway to $\bar{M}$ but at a point $\frac{1}{4}$ of the way to $\bar{M}$ that $\bar{\Sigma}_1$ state is completely bulklike. This higher $\bar{\Gamma}_1$ surface state occurred in the LCAO minority-spin bands only, and then only after the surface atomic parameters were made more negative.

To illustrate the differences between hybridized and unhybridized surface states, in Figs. 4–6 we display the $\bar{M}_3^+$, $\bar{M}_1^+$ and $\bar{X}_1^+$ surface-state wave functions as a function of z for various values of $\bar{r}$. The values of $\bar{r}$ chosen were dictated in part by nodal and symmetry considerations.[34] Orthogonalization contributions to the wave functions which would obscure the sharp $3d$ structure have intentionally been omitted. In an LCAO expansion in $4s$, $4p$, and $3d$ orbitals the $\bar{M}_3$ states consist of $d_{x^2-y^2}$ orbitals on the A planes and nothing on the B planes. The supplemented OPW surface-state wave function in Fig. 4 is completely consistent with this. Not only is there a nodal point at $\bar{r} = (\frac{1}{2}, \frac{1}{2})a$, the wave function is too small to plot everywhere in that neighborhood. The $\bar{M}_1$ states consist of s, p_z, and $d_{3z^2-r^2}$ orbitals on A planes and d_{xy} on B planes. Thus, unlike the $\bar{M}_3$ states, hybridization is not symmetry forbidden for the $\bar{M}_1$. However,

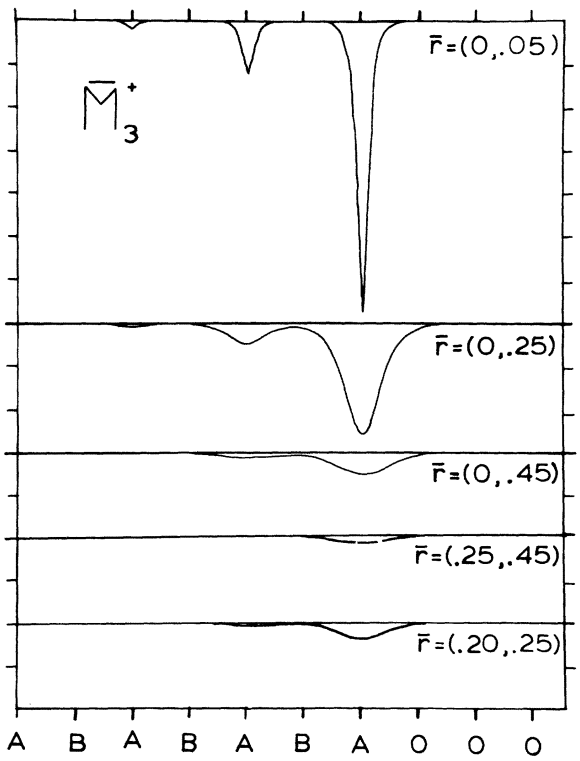

FIG. 4. Plot of the $\bar{M}_3^+$ surface state as a function of z for various values of $\bar{r}$. The tick marks on the ordinate are separated by 0.1 bohr$^{-3/2}$.

inspection of Fig. 5 reveals that the $\bar{M}_1$ surface state has little amplitude in regions far away from the ions, i.e., at $\bar{r}=(0,0.45)a$, and thus has very little s and p character hybridized in with the d. This was to be expected since the 3D band gap from which this surface state arose is between weekly interacting bands. In Fig. 6 we show the highly hybridized $\bar{X}_1$ surface state. It is interesting to note that the d-basis part of this surface state is largest on the B plane below the surface A plane and that even on the second A plane it is much larger than on the surface A plane, whereas the plane wave part of the surface state has its maximum on the surface A plane. For $\bar{r}=(0.45,0.5)a$, where we pass close to atoms on the B planes we see a huge d-like structure on the first B plane and very little plane wave structure. For $\bar{r}=(0,0)$ where we pass through A-plane atoms we see a plane-wave-like structure perturbed by some d-like structure on the surface A plane and a fairly large almost pure d-like structure on the second A plane. At $\bar{r}=(0,0.5)a$ where we avoid both A- and B-plane muffin-tin spheres we find a plane wave structure with a large broad peak whose maximum is very close to the surface A plane.

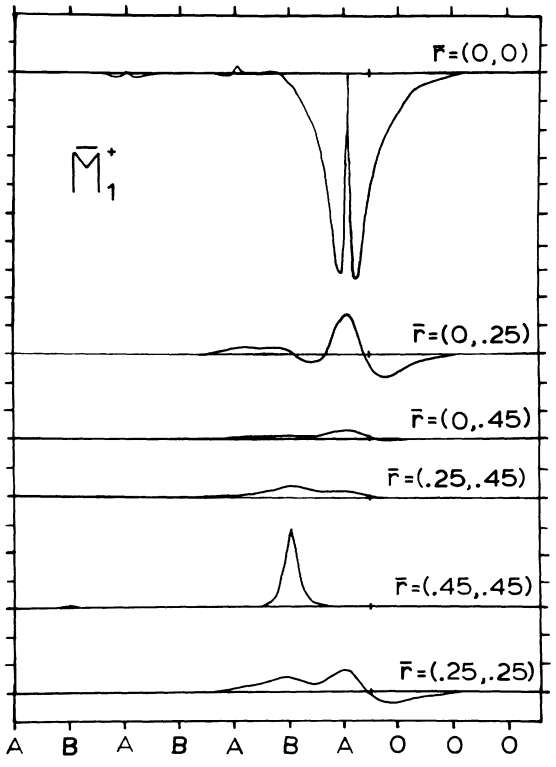

FIG. 5. Plot of the $\bar{M}_1^+$ surface state as a function of z for various values of $\bar{r}$. The tick marks on the ordinate are separated by 0.05 bohr$^{-3/2}$. The jellium surface is indicated by a tick mark on each abscissa.

Except for $\bar{M}_3$ whose $d_{x^2-y^2}$ symmetry requires charge lobes parallel to the surface, these surface states extend quite far beyond the jellium edge. Note that the two hybridized $\bar{\Gamma}_1$ surface states shown in Fig. 3 of Ref. 16 extend even farther; this is because the $\bar{M}$ and $\bar{X}$ surface states have a large component of transverse momentum and the $\bar{\Gamma}$ do not.

In Fig. 7 we show the planar average ($\bar{G}=0$ component) of the thin-film conduction-electron charge density. The contribution of every wave function to the charge density is weighted by a factor $n\alpha A/$

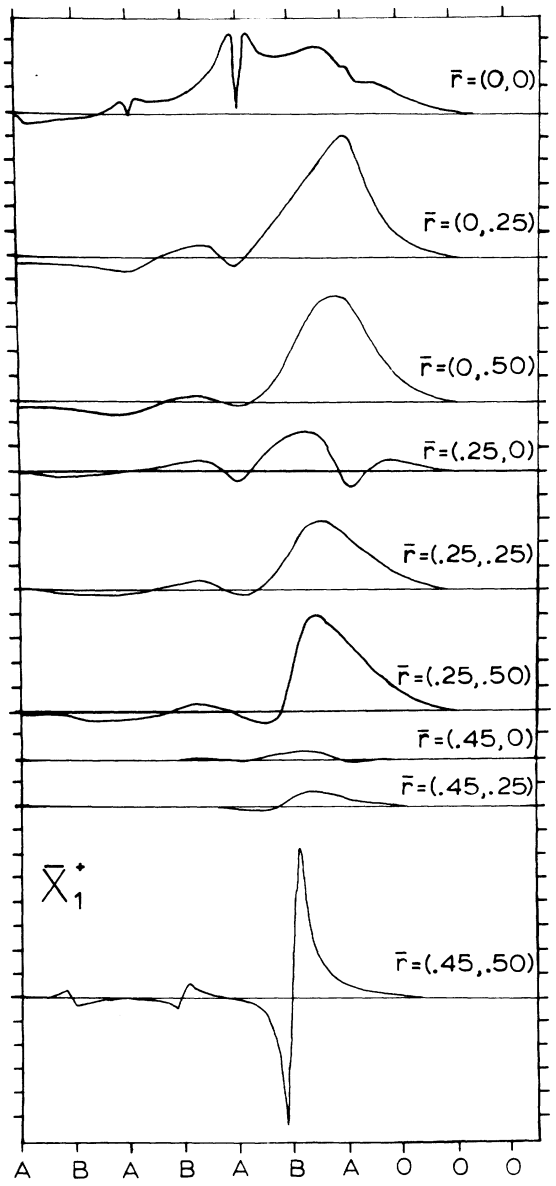

FIG. 6. Plot of the $\bar{X}_1^+$ surface state as a function of z for various values of $\bar{r}$. The tick marks on the ordinate are separated by 0.05 bohr$^{-3/2}$.

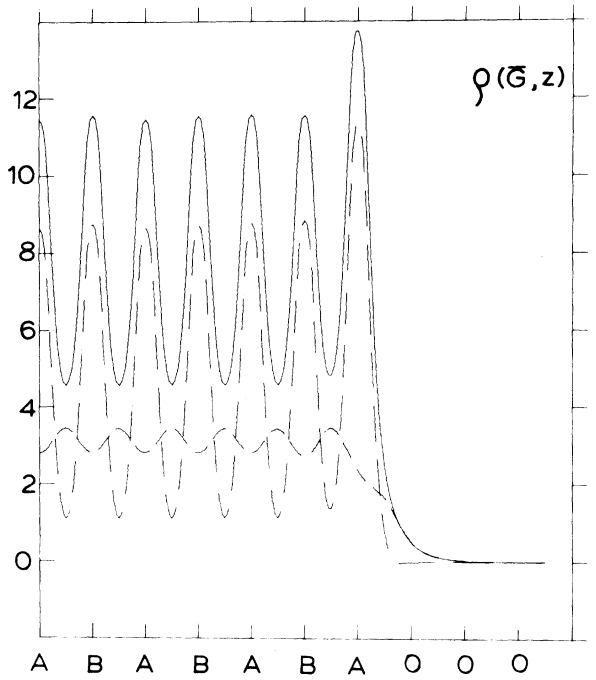

FIG. 7. Planar average of the charge density $\rho(\vec{G}=0, z)$. The plane wave contribution is indicated by short dashes, the inscribed sphere contribution by longer dashes, and the total $\rho(G=0, z)$ by the solid curve.

A_0, where nA/A_0 has previously been defined and α is an estimate of the fraction of the band, within the proximity area, that lies below the Fermi energy, i.e., $\alpha = 1$ or 0 except for states close to E_F. Our wave functions consist of plane waves plus d functions plus core functions to which the plane waves have been orthogonalized. So that upon squaring to obtain the charge density, plane-wave–plane-wave, plane-wave–core, core-core, plane-wave–d, and d-d terms are obtained. The plane-wave–plane-wave contributions to $\rho(\vec{G}=0, z)$ are indicated by the short-dashed curve which averages to about 3 electrons/atom. (Remember the plane waves have a large d component because they must make up for the fact that the d-basis functions vanish at the inscribed sphere radius.) The contributions of the spherical average of the remaining terms are indicated by longer dashes. This radial part of the charge density has a very large peak in the surface plane and, even though the plane-wave–plane-wave contribution is reduced there, leads to a very large surface plane Friedel peak in the total planar charge density. This peak is much too large and draws charge from the interior of the film. In the inner layers the charge averages only 7.7 electrons/layer, 0.3 electrons less than needed for charge neutrality. This shows that the potential with which we started was not strong enough in the center, relative to the last occupied layer and the selvage region. This is a surprising result. Our potential is based on overlapping Coulomb potentials and charge densities and is therefore already weaker in the last layer than in the interior layers.[35] Note that an *ad hoc* pseudopotential for Al constructed[3a] in much the same way as the potential here led to an essentially self-consistent charge distribution. In our ferromagnetic LCAO calculation before shifting the surface parameters we had a deficit of 0.52 electrons on the surface layer whereas the paramagnetic LCAO calculation of Desjonqueres and Cyrot-Lackmann[36] obtained a surplus of similar magnitude. Here we have a surplus of about 1.5 electrons in the surface layer and selvage region. We believe that all LCAO calculations yield too few surface electrons simply because the LCAO basis cannot account for the electronic charge in the selvage region. The difference between the ferromagnetic and paramagnetic calculations can be understood as follows. The density of states of iron is the double peaked structure[37] of Fig. 3. The surface planar density of states[6a] differs in that the two peaks are squeezed together and that some density has been transferred out of both peaks into the region in between due to the formation of surface states. Thus the higher peak occurs at lower energy and more states lie below E_F in the surface planar density of states than in the total density of states. This accounts for the large surface excess of electrons in the paramagnetic case. In the ferromagnetic case the minority-spin density of states is shifted so that E_F lies in the dip between the peaks and the majority-spin density of states is shifted so that E_F lies on the high-energy tail of the high-energy peak. Thus very few additional states lie below E_F in the surface planar density of states. One would, by this argument, expect a small surface surplus of electrons in the ferromagnetic case and one would assume our failure to obtain this small surplus in our LCAO calculation is due to the restricted nature of the LCAO basis. Of course when self-consistency is achieved, the interior of the film will be electrically neutral. Whether or not any remnant of the Friedel peak will be left remains to be seen. What we have shown here is that the response of the d electrons to the crystal surface is much stronger than that of nearly free electrons.

*Supported by NSF Grant No. DMR 73-02449-A02.

[1]G. P. Alldredge and L. Kleinman, Phys. Rev. B 10, 559 (1974).

[2]J. A. Appelbaum and D. R. Hamann, Phys. Rev. B 6, 2166 (1972).

[3]E. Caruthers, L. Kleinman, and G. P. Alldredge, (a) Phys. Rev. B 8, 4570 (1973); (b) 9, 3325 (1974); and (c) 9, 3330 (1974).

[4]J. A. Appelbaum, G. A. Baraff, and D. R. Hamann, Phys. Rev. B 12, 5749 (1975).

[5]M. Schlüter, J. R. Chelikowsky, S. G. Louie, and M. L. Cohen, Phys. Rev. B 12, 4200 (1975).

[6]D. G. Dempsey, L. Kleinman, and E. Caruthers, (a) Phys. Rev. B 12, 2932 (1975); (b) 13, 1489 (1976); and (c) unpublished.

[7]S. K. Sohn, D. G. Dempsey, L. Kleinman, and E. Caruthers, (a) Phys. Rev. B 13, 1515 (1976); (b) unpublished; and (c) unpublished.

[8]F. Forstman and V. Heine, Phys. Rev. Lett. 24, 1419 (1970).

[9]F. Forstman and J. B. Pendry, Z. Phys. 235, 75 (1970).

[10]S. J. Gurman, Surf. Sci. 55, 93 (1976).

[11]S. J. Gurman and J. B. Pendry, Phys. Rev. Lett. 31, 637 (1973).

[12]J. B. Pendry and S. J. Gurman, Surf. Sci. 49, 87 (1975).

[13]L. Kleinman, Phys. Rev. B 13, 4640 (1976).

[14]N. D. Lang and W. Kohn, Phys. Rev. B 1, 4555 (1970).

[15]R. V. Kasowski, Solid State Commun. 17, 179 (1975).

[16]E. Caruthers and L. Kleinman, Phys. Rev. Lett. 35, 738 (1975).

[17]L. Kleinman and E. Caruthers, Phys. Rev. B 10, 3213 (1974).

[18]The six pairs of planes on either side of the central plane contribute 30 even and 30 odd functions while the central plane contributes 3 even and 2 odd.

[19]F. Herman and S. Skillman, *Atomic Structure Calculations* (Prentice-Hall, Englewood Cliffs, N. J., 1963).

[20]J. C. Slater, Phys. Rev. 81, 385 (1951).

[21]We have taken $a = 2.86$Å so that the largest inscribed sphere has radius $\frac{1}{4}\sqrt{3}a = 2.3403$ a.u. Our value of r_0 was chosen to coincide with a Herman-Skillman mesh point.

[22]P. O. Löwdin, Adv. Phys. 5, 1 (1956). Note that overlapping charges or potentials in this manner yields different results for muffin tins near the surface than it does for interior muffin tins.

[23]$V^{ex}_{MT}(r)$ is needed not only as an intermediate step in calculating $V^{ex}(\bar{G}, k_3)$, but also to calculate matrix elements involving the d-basis functions and to calculate the core functions to which the plane waves are orthogonalized. In fact the $3s$ and $3p$ core functions extend beyond the inscribed sphere radius so that in order to calculate them, we extend $V_{MT}(r)$ beyond r_0. We ignore the fact that the core functions overlap, i.e., that they form a band of nonzero width.

[24]The three-dimensional $\vec{R}_j$ is a vector to the jth atom in the film. We have previously used $\bar{R}_i$ as a planar vector from the origin to the center of the ith 2D unit cell. Thus $\vec{R}_j = \bar{R}_i + \bar{\tau}_n + \vec{Z}_n$.

[25]The work function of iron is approximately 4.70 eV. See A. B. Cardwell, Phys. Rev. 92, 554 (1953).

[26]E. Caruthers and L. Kleinman, Phys. Rev. B 10, 376 (1974).

[27]The projection of one gap in Ref. 26 contains an error. The $\bar{\Sigma}_2$ gap shown running upward from an $\bar{M}$ energy of about -0.25 Ry should pinch off about $\frac{1}{8}$ of the way to $\bar{\Gamma}$ from $\bar{M}$ and then reopen. Two 3D levels having different symmetry (G_2 and G_4) both project to give $\bar{\Sigma}_2$ bands and these cross in 3D.

[28]J. H. Wood, Phys. Rev. 126, 517 (1962).

[29]R. A. Tawil and J. Callaway, Phys. Rev. B 7, 4242 (1973).

[30]The $\bar{Y}_1$ and $\bar{Y}_2$ symmetries are interchanged under interchange of the A and B planes. Therefore, in the bulk where A and B sites are indistinguishable, the $\bar{Y}_1$ and $\bar{Y}_2$ states must occur as degenerate pairs.

[31]In a thick film an $\bar{M}_5$ surface state is therefore fourfold degenerate.

[32]We examined this surface state at $\bar{k} = (2\pi/a)(\frac{7}{16}, \frac{7}{16})$ which is not point on our 2D BZ mesh but is midway between $\bar{M}$ and the place where the gap pinches off.

[33]The $\bar{M}_{1,4}$ continuum is projected from a D_1 band and the $M_{2,3}$ from a D_2 band which are degenerate at P with P_3 symmetry. If P_3 is the highest point in both bands then the tops of the two M continua are degenerate. In the 13-layer film the degeneracy of the $\bar{M}_2$ surface-state pair was split by 0.00014 Ry and it lay 0.0014 Ry above the highest state in the $M_{1,4}$ continuum.

[34]The $\psi_{\bar{M}}(x, y, z)$ are symmetric under interchange of x and y. Both the $\bar{M}_3$ and M_1 states have nodes for $x = \pm\frac{1}{2}a$ or $y = \pm\frac{1}{2}a$; in addition the $\bar{M}_3$ states have nodes for $x = y$. The $\bar{X}_1$ states have nodes for $x = \pm\frac{1}{2}a$.

[35]This may be verified by noting that the $1s$, $2s$, and $2p$ core eigenvalues are about 0.018 Ry less negative for the surface ions.

[36]M. C. Desjonqueres and F. Cyrot-Lackman, J. Phys. (Paris) 36, L45 (1975); J. Phys. F 5, 1368 (1975).

[37]The peaks in the density of states for a thicker film sampled at more points in the 2D BZ are somewhat sharper than those of Fig. 3.